Downscaling Gridded DEM using the Hopfield Neural Network

Journal:	*Journal of Selected Topics in Applied Earth Observations and Remote Sensing*
Manuscript ID	JSTARS-2018-00862
Manuscript type:	Regular
Date Submitted by the Author:	24-Sep-2018
Complete List of Authors:	Nguyen, Quang Minh; Hanoi University of Mining and Geology, Faculty of Geomatics and Land Administration La, Phu Hien; Hanoi University of Mining and Geology, Faculty of Geomatics and Land Administration Pham, Thanh Thao; Hanoi University of Mining and Geology, Faculty of Geomatics and Land Administration Nguyen, Thi Thu Huong; Hanoi University of Mining and Geology, Faculty of Geomatics and Land Administration Lewis, Hugh; University of Southampton, School of Engineering Sciences; Atkinson, Peter; Lancaster University, Faculty of Science and Technology; Queen's University of Belfast, School of Geography, Archaeology and Palaeoecology
Keywords:	Hopfield networks, Remote sensing

Downscaling Gridded DEM using the Hopfield Neural Network

Nguyen Quang Minh, Nguyen Thi Thu Huong, La Phu Hien, H.G. Lewis, P.M. Atkinson

Abstract— **In this paper, a new model for downscaling of a digital elevation model in grid form (gridded DEM) is proposed. The downscaling model works by minimizing the local semivariance as a goal, and by matching the original coarse spatial resolution elevation value as a coherence constraint. The approach was coded into the Hopfield neural network (HNN) model in which each pixel of the original coarse DEM is divided into m×m sub-pixels, represented as network neurons. The elevation of each sub-pixel is derived iteratively (i.e. optimized) based on minimizing the local semivariance under the elevation coherence constraint. A simple linear activation function was used in this HNN model. The proposed model was tested against two commonly applied alternative benchmark methods (bilinear resampling and bi-cubic resampling) via an experiment using both degraded and sampled datasets at 20 m, 60 m and 90 m spatial resolutions. The evaluation of the algorithms was accomplished comprehensively with visual and quantitative assessments. The visual assessment process was based on direct comparison of the same topographic features in different downscaled images, scatterplots and profiles. The quantitative assessment was based on the most commonly used parameters for DEM accuracy assessment such as root mean square errors (RMSEs), linear regression parameters m and b, and correlation coefficient R. Both visual and quantitative assessment revealed a much greater accuracy of downscaled DEMs when using the HNN approach for increasing the spatial resolution of the gridded DEMs.**

*Index Terms—*Digital Elevation Model, Downscaling, Hopfield Neural Networks.

I. INTRODUCTION

THE he spatial resolution of a gridded DEM affects both the information content and the accuracy of the data and, potentially, of many other secondary data products [1], [2]. Examples include the well-known effects of spatial resolution on the spatial properties of DEM and other spatial data [3], [4], and more specifically on slope and aspect [5], [6], , watershed boundary delineation and the accuracy of SWAT schemes [7], [8], water run-off models [9], [10], three dimensional modelling of landscapes [11], local slope, plan curvature, drainage area

[12], [13], soil survey results and soil moisture [14], [15]. All of the above-mentioned studies showed that DEMs with a finer spatial resolution can produce more informative and potentially more accurate results.

Gridded DEMs with fine spatial resolution and high accuracy can be acquired using remote sensing and airborne LiDAR technology, ground surveying or photogrammetry [16], [17]. Airborne LiDAR enables the acquisition of data with a very high density of 3-dimensional coordinate points and, therefore, production of a DEM with sub-meter spatial resolution. Airborne LiDAR-derived DEMs have been used in many different applications, some of which require very fine spatial resolution and very high accuracy [18]. Although being capable of generating a fine spatial resolution DEM, airborne LiDAR technology has some challenges such as the very large amount of data storage required and high computing capacity for data processing. Compared with airborne LiDAR, other methods for fine spatial resolution DEM acquisition such as ground surveying and photogrammetry are more time consuming and labour intensive [19]. Hence, if the resolution of the DEM can be increased using algorithms, it is possible to save the time and labour cost by fine resolution DEM generating. Additionally, the improvement in accuracy and resolution of DEM though a simple algorithm is an added product for any available source of DEM data.

Potentially, raster DEM data can be downscaled using several resampling approaches [20]. The most commonly used approaches for downscaling DEMs are nearest neighbor, bilinear and bi-cubic interpolation [21], [22]. A research by Dixon and Earls [23] used the simple nearest neighbour resampling to increase the resolution of DEMs and compare the effects of results to the DEM's products such as stream flow, watershed, delineations, number of sub-basins and slopes. It was showed that the simple resampling of DEM does not increase the accuracy of DEMs greatly, or in the other hand, the resampling methods in this case did not create new significant information that is not available at the original resolution of DEM [24]. However, an experiment by Shi et. al. [22] showed

that downscaling using bilinear resampling can increased the accuracy of DEMs in term of root mean square error (RMSE) with a suitable value of re-sampling ratio r. Jana et. al. [25] and Jordan [26] increased the accuracy of DEM from the raster contour data and ridgeline elevation. However, these methods used additional information from raster channels to correct the elevation of DEM's cells. Similarly, the accuracy and resolution of gridded DEM can be increased using geostatistical methods and sets of additional high accurate elevation data points [27], [28]. Other methods include B-spline resampling and the filtering method used in a patent by Atkins et al. [29]. All of these researches suggested that the downscaling of raster data can potentially increase the spatial resolution of these data for use as a gridded DEM.

Sub-pixel mapping is a technique used to predict land cover class at the sub-pixel scale (i.e., at a spatial resolution that is finer than the original input data) using a soft-classified land cover proportions image as input [30]. In terms of geographical scaling, sub-pixel mapping approaches are downscaling techniques which use the soft-classified land cover proportions as a pixel-level constraint and maximize some goal functions (e.g., the spatial dependence between sub-pixels) to increase the spatial resolution [31]. Several sub-pixel mapping techniques have been developed such as the sub-pixel swapping [32], [33], Markov random field [34], geospatial based method (Atkinson et al., 2008) and Hopfield neural network (HNN) approaches [35], [36], [37], [38], [39]. The HNN technique has previously been modified for smoothing and increasing the spatial resolution of raw multispectral remotely sensed imagery [40]. Because remote sensing images and gridded DEMs are both provided in the raster data model, it is expected that a new approach developed based on the idea of HNN approach for remote sensing images may be applied for gridded DEM due to the similar feature of these two types of data. This paper explores the potential for development and application of the new HNN model to the task of downscaling DEM imagery. Specifically, a new model of HNN was developed to increase the resolution and accuracy of gridded DEM and tested with different sources of elevation data.

II. METHOD

A. HNN approach for sub-pixel mapping

The model proposed here for increasing the spatial resolution of a gridded DEM is based on the idea of the HNN designed for sub-pixel mapping [35], [41]. In the HNN for sub-pixel mapping, an original pixel is divided into m×m sub-pixels and each sub-pixel is represented by a neuron in the HNN. This particular model is based on an area proportion constraint and two goal functions. The proportion constraint ensures that the total number of sub-pixels of each land cover class is equal to the number of sub-pixels assigned by the soft-classified land cover proportion. The goal functions play the role of a spatial dependence engine, which increases the tendency of adjacent sub-pixels to belong to the same land cover class.

In the HNN used for sub-pixel mapping, the output vij of a neuron (sub-pixel) (i, j) is:

$$v_{ij} = g(u_{ij}) = \frac{1}{2(1+tanh\lambda u_{ij})} \tag{1}$$

here $g(u_{ij})$ is an activation function of each neuron, u_{ij} is the input value of each neuron and λ is steepness value, which is defined empirically as 100.

The input value u_{ij} is determined at the time t as

$$u_{ij}(t) = u_{ij}(t - dt) + \frac{du_{ij}}{dt} dt \tag{2}$$

where, dt is time step, $u_{ij}(t - dt)$ is the output value at the time $(t - dt)$ and du_{ij}/dt is defined as follows:

$$\frac{du_{ij}}{dt} = \frac{dE_{ij}}{dv} \tag{3}$$

where, E is the energy, defined as $E = $ Goals + Constraint and

$$\frac{dE_{ij}}{dv} = \left(\sum_e^K \frac{dGoal_e}{dv} + \frac{dConstraint}{dv} \right) \tag{4}$$

where, K is the number of Goal functions. Depending on the specific application, the goal and constraint functions can be modified for optimization. In Tatem et al. [35], the Goal functions are the two *Goal functions* for spatial dependence maximization, and the Constraint Functions comprise an *Area Constraint function* used for retaining the area proportions predicted by the soft-classification and a *Multi-class Function* which ensures that a sub-pixel belongs to only one class. In Nguyen et. al. [41] *Panchromatic Constraint Function* was added to the HNN model of Tatem et. al. [35] to increase the accuracy of the sub-pixel mapping results.

The running of the HNN in the above cases is terminated when the total energy E of the HNN reaches a minimum value determined as

$$E = \sum_i \sum_j \left(\sum_f \left(k_f v_{ij}^{Goal_f} \right) + \sum_g \left(k_g v_{ij}^{Constraint_g} \right) \right) = min$$

Or: $E(t) - E(t - dt) = 0 \tag{5}$

B. 2.2. Proposed HNN approach for gridded DEM downscaling

The new proposed approach is based on the assumption that the elevation of each sub-pixel must be close to its adjacent sub-pixels (spatial dependence assumption). The realization of spatial dependence in this case is calculated using the semivariance, which can be defined as

$$\gamma(h) = \frac{1}{2N(h)} \sum_1^{N(h)} [v_{ij} - v_{ij+h}]^2 \tag{6}$$

where $\gamma(h)$ is the semivariance value at lag distance h (i.e., ignoring direction), h is the distance between a pair of data points v_{ij} and v_{ij+h}, and $N(h)$ is the number of pairs of data points. If the points are spatially dependent, the semivariance will be small at small value of h. In other words, there is greater spatial dependence when there is a large difference between the *a priori* variance (maximum fitted semivariance at large h) and the smallest semivariance at small h. Thus, minimizing the semivariance at small h (at the sub-pixel scale) effectively maximizes the spatial dependence, that is, creates the greatest amount of spatial structure in the DEM at fine spatial resolution. The minimum value of semivariance can be defined based on the derivative as

$$\frac{\partial \gamma(h)}{\partial v} = 0 \tag{7}$$

and,

$$\frac{\partial \gamma(h)}{\partial v} = \frac{1}{2N(h)} \sum_1^{N(h)} (2v_{ij} - 2v_{ij+h}) = v_{ij} - \frac{\sum_1^{N(h)} v_{ij+h}}{N(h)} \tag{8}$$

So, from equation (7), it is possible to achieve an expected output value of

$$v_{ij}^{expected} = \frac{\sum_1^{N(h)} v_{ij+h}}{N(h)} \qquad (9).$$

The change in elevation of each sub-pixel from the spatial dependence maximization operation is

$$du_{ij}^{sd} = v_{ij}^{expected} - v_{ij} \qquad (10).$$

This means that the expected value of data points v_{ij} is the average of the values of all data points with lag distance h (v_{ij+h}). In this model, for a gridded DEM, the data points with smallest h are the eight pixels surounding the pixel v_{ij}. This function can be called as the *spatial dependence maximization function*. Similar to two Goal functions in the HNN model proposed by Tatem et al. [35], the *spatial dependence maximization function* also maximizes the spatial dependence between the adjacent sub-pixels. However, the difference between these function is that while the Goal functions of Tatem et al. increase the value of central sub-pixel to 1 or reduce the value of central sub-pixel to 0, the *spatial dependence maximization function* in the new HNN model increases or reduces the output value of central sub-pixel to the averaged elevation of eight surrounding sub-pixels.
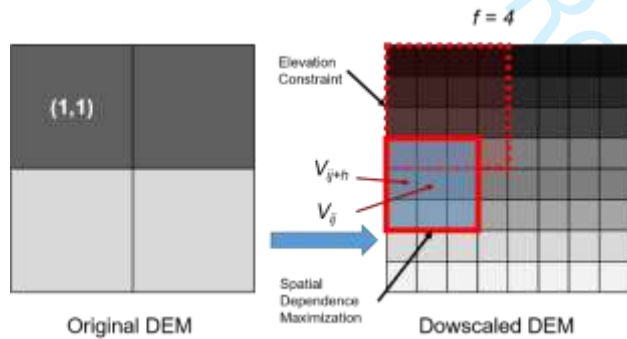

Fig. 1. Downscaling of grid DEM by a factor of 4

The proposed model developed for downscaling a grid DEM is presented in Fig. 1 for the example case of a DEM with 2×2 pixels sizes. A pixel in the original DEM is divided into 4×4 sub-pixels in the new DEM (zoom factor $f = 4$). So the original image of 2×2 pixels is resampled to an image of 8×8 sub-pixels. Each sub-pixel is represented by a neuron in the HNN model where the initial value is the elevation value of the pixel in the original DEM (or may be assigned randomly). According to Formula (10), the expected elevation for each sub-pixel is equal to the average of the 8 surounding sub-pixels (based on the spatial dependence maximization function using a 3×3 window).

If the spatial dependence maximizing function is the only function used in the model, the elevation of all sub-pixels in the new DEM will be finally the same and the elevation values of the coarse original DEM will not be preserved. To resolve this problem, a simple constraint function is used. The principle of this constraint is perfect coherence between scales; the elevation of a pixel of the DEM represents the averaged elevation of all points within that pixel. That means the average elevation of all sub-pixels located within a pixel of the original

DEM must be equal to the elevation of that original pixel. For example, the average of the elevation of all sub-pixels within the area of the pixel (1,1) of the original image in Fig. 1 must be equal to the elevation of the pixel (1,1).

$$du_{ij}^{ep} = Elevation_{x,y} - \frac{\sum_{(x-1)\times m}^{x\times m} \sum_{(y-1)\times m}^{y\times m} v_{pq}}{m\times m} \qquad (11),$$

where $Elevation_{x,y}$ is the elevation value of the pixel (x, y) in the original image, v_{pq} is output (elevation) value of the sub-pixel (p, q) in the newly generated image covered by pixel (x, y), and m is the zoom factor. If the average of the elevation values of all sub-pixels within a pixel is smaller than the $Elevation_{x,y}$, then a value is added to the elevation value v_{pq} of all sub-pixels covered by pixel (x, y). In contrast, when the average of the elevation values of all sub-pixels within pixel (x, y) is larger than the $Elevation_{x,y}$, a value is subtracted from the output value v_{pq} of the neuron (p, q).

Then an input value of each neuron (sub-pixel) can be calculated based on Formula (2) with the value du_{ij}/dt as

$$\frac{du_{ij}}{dt} = \frac{dE_{ij}}{dv} = du_{ij}^{sd} + du_{ij}^{ep} \qquad (12).$$

The output value v_{ij} of each neuron is then calculated using an activation function $g(u_{ij})$. However, in this new model, the activation function $g(u_{ij})$ is not the same as in Equation 1 because it is not used for pushing the output value of the neurons to 0 or 1 as in the case of HNN for sub-pixel mapping. Instead, a linear activation function as presented in a Tank and Hopfield research [42] was used in this new approach as

$$v_{ij} = g(u_{ij}) = a \times u_{ij} + b \qquad (13)$$

where, $a = 1$ and $b = 0$ in this model.

The HNN network runs until the energy is minimized as

$$E = \sum_i \sum_j (du_{ij}^{sd} + du_{ij}^{ep}) = min \qquad (14)$$

or, the $E(t) - E(t - dt) = 0$, where $(t - dt)$ and t are two consecutive iterations of the Hopfield Neural Network.

III. ASSESSMENT OF THE ALGORITHM

A. Reference and testing data

Two types of data were used to evaluate the proposed algorithm. The first type of data was *degraded* coarse DEMs which were calculated from the reference DEMs at fine resolution using nearest neighbour (or averaging method) to make an error-free data for algorithm testing. These data alone may be enough to assess the algorithm but it may lead to a skepticism because they were not *real* DEMs. The real DEMs, as someone may argue, are mostly sampled from point elevation or contour data rather than being averaged from the elevation of sub-pixels within a footprint of the original pixel. Actually, the elevation of a pixel of the DEM represents the elevation of the surface covered by this pixel so it must be the averaged elevation of this surface. The interpolation algorithms are used to estimate this representing elevation from point or contour data so the elevation of a pixel in the *real* grid DEMs is actually the averaged elevation of all points within the footprint of this pixel with some estimation errors. To implement more comprehensive evaluation of the new HNN algorithm, the

sampled (real) DEMs generated by interpolating point elevation and contour data were used.

The spatial resolution for all four testing DEM datasets in this paper was selected between 5 m and 90 m and, accordingly, the zoom factor values are 3 or 4. There are two reasons for this selection of the spatial resolution. The first reason is because most of currently available sources of grid DEM data are at this range of resolution. The second and more important reason is that the increasing in accuracy of the data at these spatial resolutions is useful for many applications. Finer resolution grid DEM data may be obtained from airborne LiDAR or 3D Laser scanners but they are accurate enough for most of the applications therefore the increasing in accuracy or resolution of these types of data are actually not necessary and meaningful.

The first set of degraded DEM data covered an area of about 3.5 km by 3.5 km and were acquired at Yen Thanh District, Nghe An Province, in North Central Vietnam. The area is located at 18º 58' 57.03" N, 105º 22' 44.87" E, about 45 km from Vinh City. This DEM was produced from topographic maps at the scale of 1:10000. The spatial resolution of the original DEM is 20 m (Fig. 2(a)) and this was degraded to 60 m by averaging the elevation value of 20 m pixels within the footprint of the degraded 60 m (Fig. 2(b)).

The second downscaled DEM dataset was provided by the Shuttle Radar Topography Mission (SRTM) of the USGS Earth Explorer (http://earthexplorer.usgs.gov/) (Fig. 3(a)). This dataset covered the same area as the first DEM but with a spatial resolution of 30 m. This was also degraded to 90 m to create a second set of test data for the HNN algorithm (Fig. 3(b)).
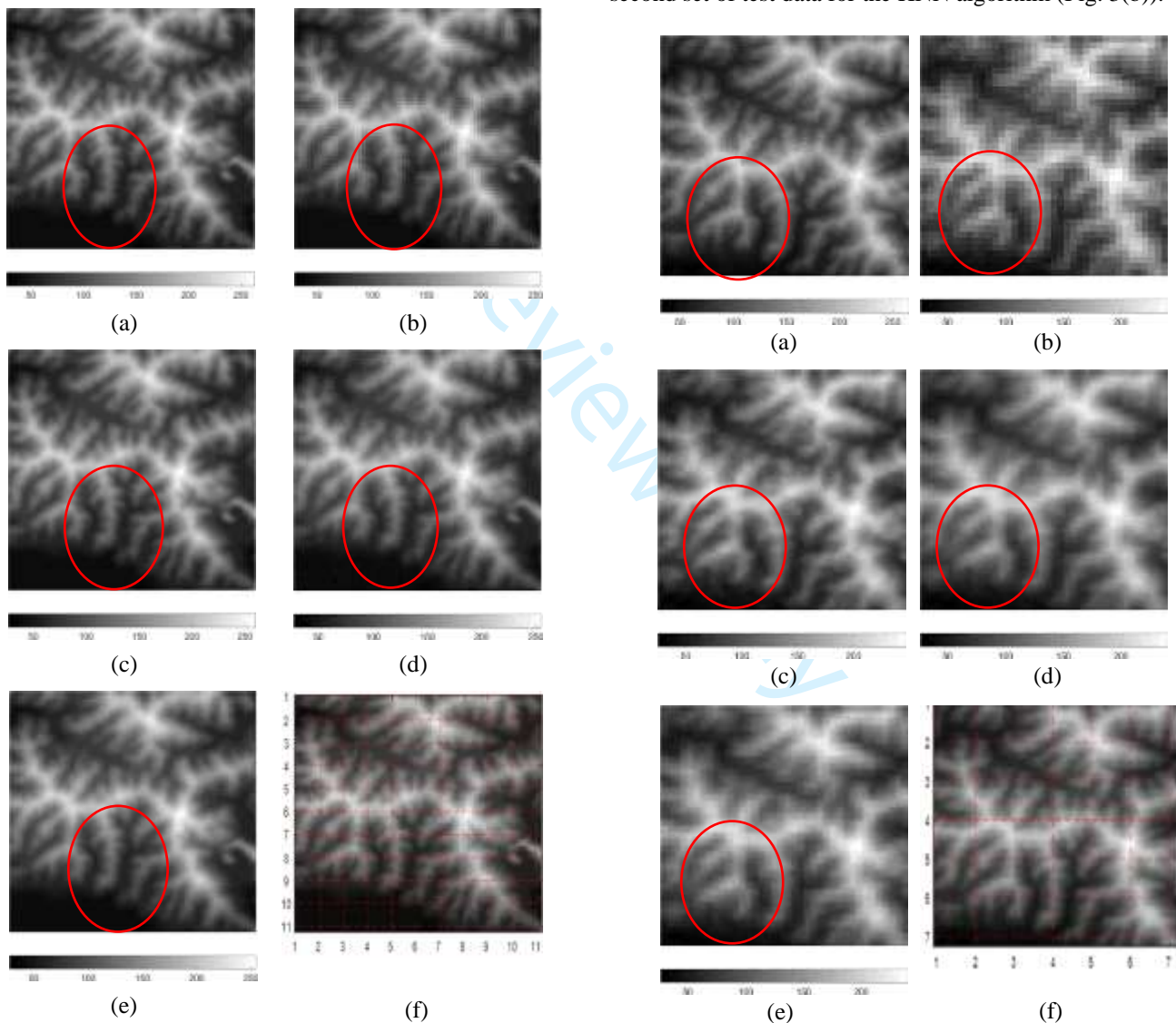
(a)

(b)

(c)

(d)

(e)

(f)

Fig. 2. Downscaling of DEM from 60 m to 20 m spatial resolution. (a) Reference DEM at 20 m resolution; (b) Degraded DEM at 60 m resolution (note: this forms the only input to the algorithms); (c) HNN downscaled DEM at 20 m resolution; (d) DEM at 20 m using bilinear resampling; (e) DEM at 20 m resolution using bi-cubic resampling; and (f) the positions of profiles for DEM accuracy evaluation.

Degraded DEMs

(a)

(b)

(c)

(d)

(e)

(f)

Fig. 3. Downscaling of DEM from 90 m to 30 m spatial resolution. (a) Reference DEM at 30 m resolution; (b) Degraded DEM at 90 m resolution (note: this forms the only input to the algorithms); (c) HNN downscaled DEM at 30 m resolution; (d) DEM at 30 m resolution resulted from bilinear resampling; (e) DEM 30 m resolution resulted from bi-cubic resampling; and (f) the positions of profiles for DEM accuracy evaluation.

TABLE I
ACCURACY ASSESSMENT BASED ON ASPRS ACCURACY STANDARD FOR DIGITAL GEOSPATIAL DATA

| Dataset and standards | Absolute Accuracy | | | Appropriate Contour Interval Supported by the RMSEz value |
	$RMSE_z$ Non-Vegetated (cm)	NVA at 95% Confidence Level (cm	VVA at 95th Percentile (cm)	
Mai Pha, Langson DEM	48.3	1.449-meter	1.449	1.449-meter
Standard ASPRS class VIII (66.7-cm)	66.7	2-meter	200	2-meter

generate a gridded DEM dataset at 5 m spatial resolution for use as a reference, as can be seen in Fig. 4(a). The accuracy of reference DEM was assessed based on the ASPRS Accuracy Standard for Digital Geospatial Data [43], [44] with a set of 234 validation points. The results of assessment (Table 1) showed that the quality of the reference DEM is slightly better than that of 66.7-cm ASPRS DEM Class and Class VIII of ASPRS 1990 Standards [44] with $RMSE_z$ of 48.3 cm and the Appropriate Contour interval of 1.449-meter. The coarse DEM at 20 m spatial resolution was created using the same interpolation algorithm from the point data (Fig. 4(b)). This coarse 20 m DEM was used as input for the HNN algorithm to make 5 m DEM and this result was compared with 5 m DEM reference data.
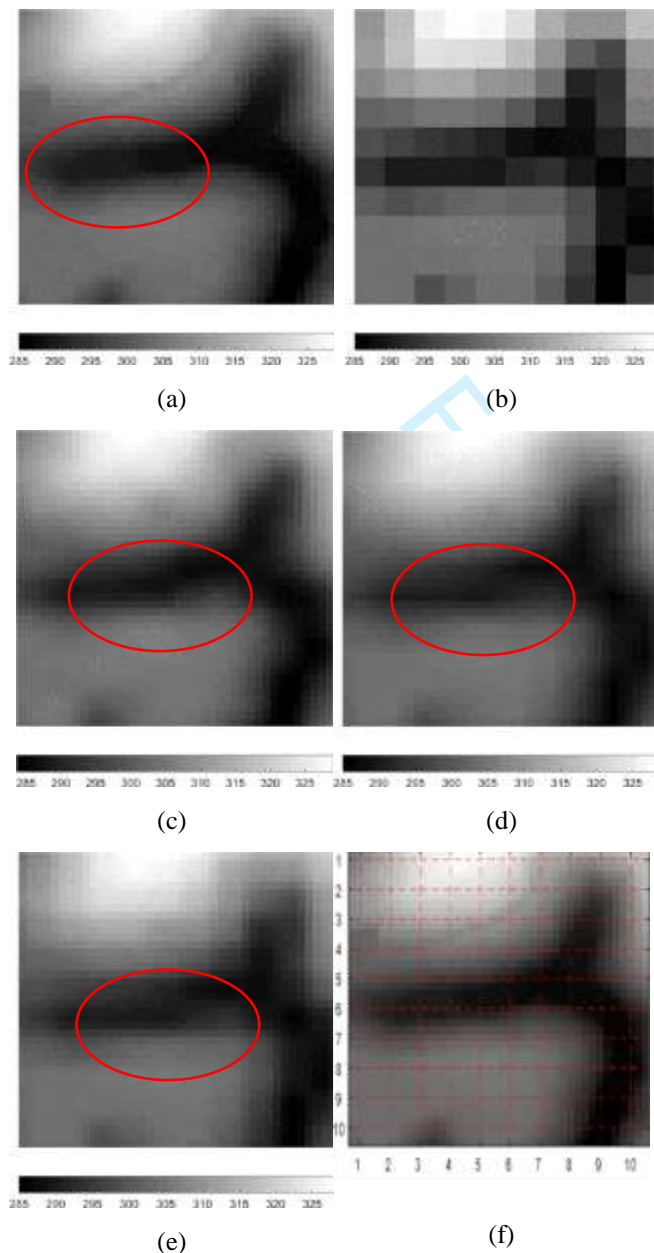

Fig. 4. Downscaling of DEM data from 20 m to 5 m spatial resolution. (a) Reference DEM data at 5 m resolution; (b) Degraded DEM data at 20 m resolution (note: this forms the only input to the algorithms); (c) HNN downscaled DEM at 5 m resolution; (d) DEM at 5 m resolution resulted from bilinear resampling; (e) DEM at 5 m resolution resulted from bi-cubic resampling; and (f) the positions of profiles for DEM accuracy evaluation.
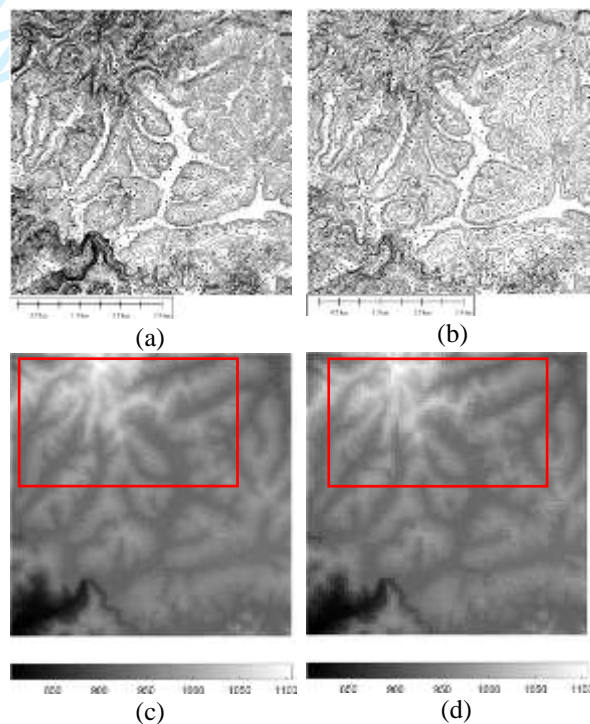
Sampled DEMs

The first sampled dataset was acquired using ground surveying in Lang Son Province of Vietnam. The area of the test field is about 200 m by 200 m in Mai Pha Ward, Lang Son City which is about 150 km from Hanoi. A set of 533 measured elevation points were used with Kriging interpolation to
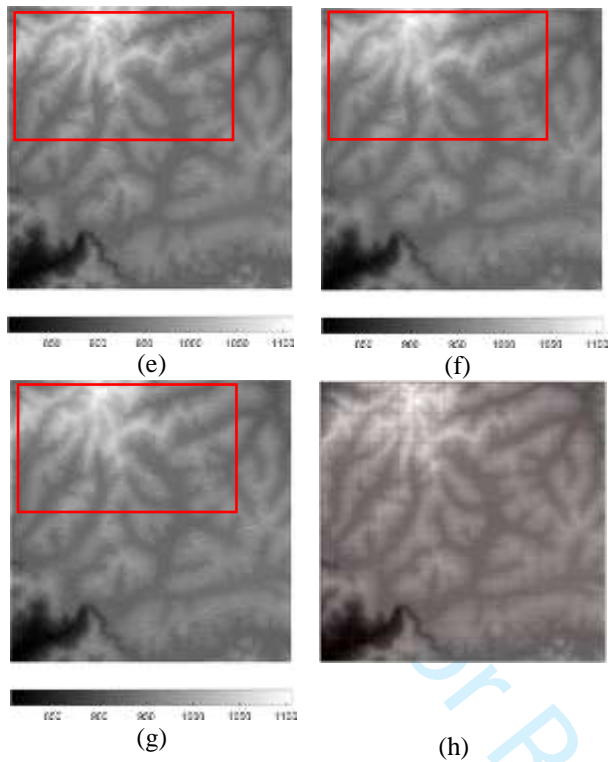
Fig. 5. Downscaling of DEM data from 90 m to 30 m spatial resolution. (a) Contour data at 5 m interval; (b) Contour data at 10 m interval; (c) Reference DEM data at 20 m resolution (created from 5 m internal contour data); (d) Input DEM data at 90 m resolution (created from 10 m internal contour data) (note: this forms the only input to the algorithms); (e) HNN downscaled DEM at 30 m resolution; (f) DEM at 30 m resolution resulted from bilinear resampling; (g) DEM at 30 m resolution resulted from bi-cubic resampling; and (h) the positions of profiles for DEM accuracy evaluation.

B. Reference and testing data

1) Results and assessment methods

To test the proposed algorithm, the DEMs with coarser spatial resolution were used as an input to the proposed algorithm to produce DEMs at the same resolution of reference data using the bilinear, bi-cubic resampling and the HNN downscaling algorithms. A computer program for the HNN downscaling was created using Visual Basic 6 platform. The running of the HNN downscaling program was performed by a computer with Intel Pentium 5 Processor and 8 GB Ram. For Lang Son dataset, the running time was 2 seconds after 53 iterations. For the other three testing data, the running time were from 5 minutes to 7 minutes, depending on the sizes of the DEMs. Results of these downscaling for four datasets are presented in Fig. 2, Fig. 3, Fig. 4 and Fig. 5.

The assessment was implemented based on both visual comparison of the resulting DEMs from the three different methods and quantitative evaluation using the parameters which were usually used for DEMs' accuracy assessment such as RMSE [45], coefficient of determination [46], the linear regression parameters, and the elevation profiles [47], [45]. Visual assessment of the results was carried out in several approaches. The first approach is direct visual comparison of the DEM images, especially comparison of the same topographical features in different images. The second approach is to analyse the scatterplots between the elevation

values the pixels of reference DEMs and the elevation values of the coresponding pixels of the HNN downscaled DEM, bilinear and bi-cubic resampled DEMs as in Fig. 7, Fig. 8, Fig. 9, and Fig. 10. Another approach which was used in many previous research on DEMs evaluation is comparing the cross-sections (profiles) of the resulted downscaled DEMs [47], [45]. These profiles present the matching between the surfaces formed by the reference fine spatial resolution DEM and the surfaces formed by DEM at coarse spatial resolution, DEMs generated by bilinear, bi-cubic resampled and the HNN downscaling algorithms and therefore enable the evaluation of the effects of the algorithms on different forms of terrain and topographical features. The locations of the profiles for the four datasets are presented in Fig. 2(f), Fig. 3(f), Fig. 4(f) and Fig. 5(h).

The quantitative assessment was implemented mainly based on the RMSEs for whole images and each profiles of the Nghe An (20 m spatial resolution and 30 m spatial resolution), Lang Son and Dac Ha datasets as presented in Table 4, Table 2, Table 3, and Table 5, respectively. Together with the RMSEs, the linear regression coefficents such as slope coefficient m, the intercept coefficient b, and the correlation coefficent R were used to assess the matching between the downscaled DEMs from the HNN downscaling, biliner and bi-cubic resamplings and the reference DEMs for 4 datasets as in Table 2, Table 3, Table 4, Table 5 and Table 6.

2) Visual assessment

Visual comparison showed that the resulting DEMs from the newly proposed HNN method are visually more similar to the reference DEM than the coarse spatial resolution DEMs and the DEMs generated by the bilinear and bi-cubic resampling methods for both degraded and sampled datasets. The improvement in visual similarity between the resulted downscaled DEMs and reference DEM is seen clearly when comparing between the 20 m and 30 m DEMs in degraded datasets in Nghe An (Fig. 2 and Fig. 3) and 5 m and 30 m resampled DEMs with reference DEMs (Fig. 4 and Fig. 5). While the images of original coarse resolution DEMs and the DEMs by resampling methods, especially the images created by bi-cubic resampling, were blurred with noises and the shapes of terrain features in these images look distorted, the images of HNN downscaled DEMs in Fig. 2(c), Fig. 3, Fig. 4(c) and Fig. 5(e) look noise-free and very similar to the reference DEMs in Fig. 2(a), Fig. 3(a), Fig. 4(a), and Fig. 5(c). The most clearly improvement of reconstruction of the shapes of terrains from coarse resolution data can be seen in the marked areas in Fig. 2, Fig. 3, Fig. 4, and Fig. 5.

The comparison of the surfaces of the resulting DEMs using profiles in Fig. 6 reveals a clearer advantage of the HNN downscaling method over the original coarse resolution DEM and the DEMs created by resampling methods. In this figure, the elevation profiles of the HNN downscaled DEMs are closer to the profiles of reference DEMs than those of the bilinear and bi-cubic resampled DEMs for both degraded and sampled datasets. This is most clearly seen in the 5 m Lang Son dataset as in Fig. 6(c) (a row profile) and Fig. 6(g) (a column profile) in the places such as tops of the hills or bottoms of valleys. In these images, it is possible to observe that the surfaces from the

bilinear and bi-cubic resampling methods are closer to the original coarse spatial resolution surface while the surface formed by the HNN downscaled DEM are closer to the 5 m reference surface. The HNN downscaling method performed much more accurately than the bilinear and bi-cubic resampling methods for more extreme elevation features such as the tops of ridges and hills or bottoms of the valleys, especially for V-shaped valleys and sharp ridges and hills. This can be explained by the effects of the *elevation constraint* that helps to reduce or increase the elevation at such points while the *spatial dependence maximization function* makes the elevations of the adjacent sub-pixels change gradually as in the real terrain.
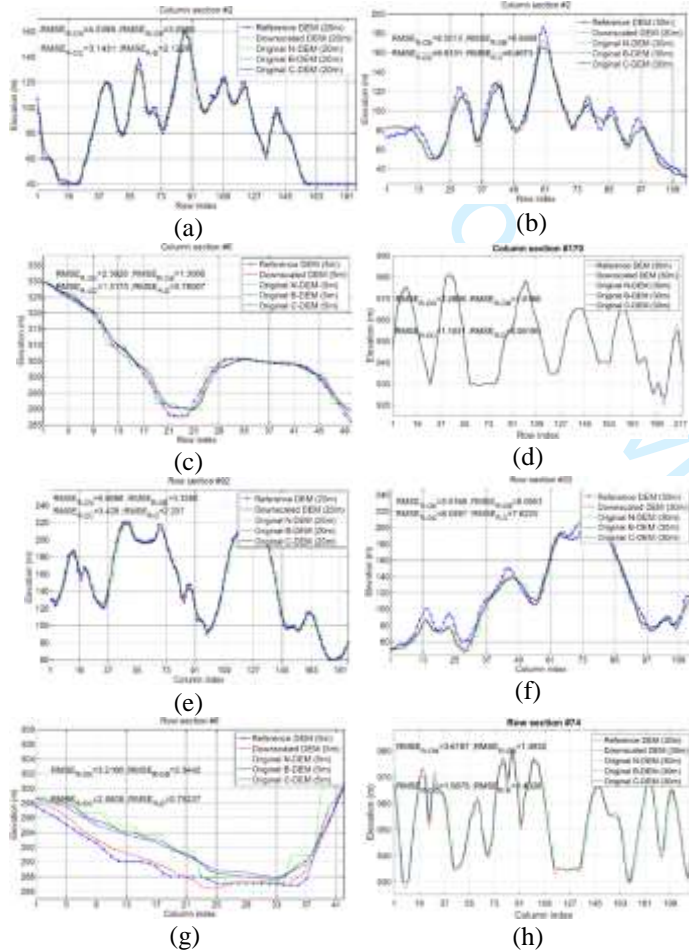
(a)   (b)

(c)   (d)

(e)   (f)

(g)   (h)

Fig. 6. Comparison of reference surface (reference DEM), HNN downscaled surface (downscaled DEM), original coarse resolution surface (original N-DEM), bilinear (original B-DEM) and bi-cubic (original C-DEM) resampled surfaces based on profiles: (a) a column profile for 20 m degraded dataset in Nghe An; (b) a column profile for 30 m degraded dataset in Nghe An, (c) a column profile for 5 m sampled dataset in Lang Son; (d) a column profile for 30 m sampled dataset in Dac Ha; (e) a row profile for 20 m degraded dataset in Nghe An; (f) a row profile for 30 m degraded dataset in Nghe An; (g) a row profile for 5 m sampled Lang Son dataset; a row profiles for 30 m sampled dataset in Dac Ha, Vietnam

(a)   (b)

(c)   (d)

Fig. 7. Scatterplots of the reference fine spatial resolution DEM against the downscaled DEM for the degraded 20 m Nghe An dataset test: (a) reference DEM and coarse degraded DEM (N-DEM), (b) the reference DEM and the HNN downscaled DEM (D-DEM), (c) the reference DEM and the bilinear resampled DEM (B-DEM), (d) the reference DEM and the bi-cubic resampled DEM (C-DEM).

(a)   (b)

(c)   (d)

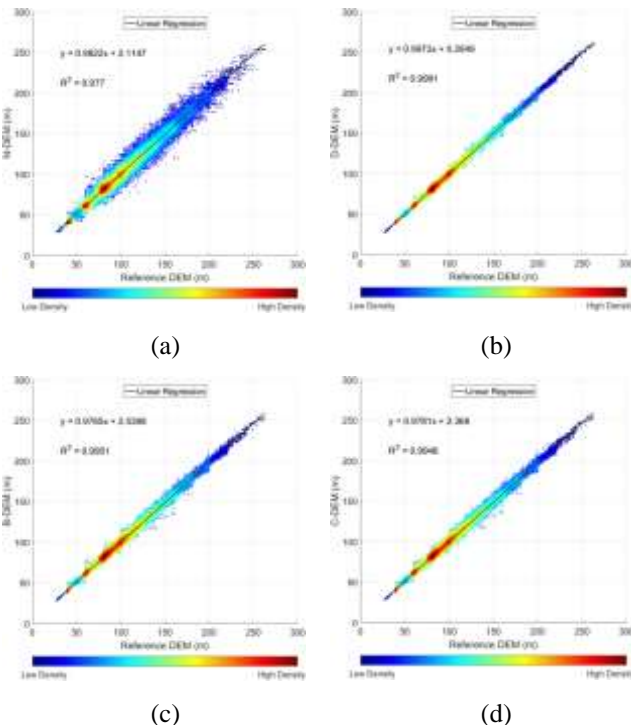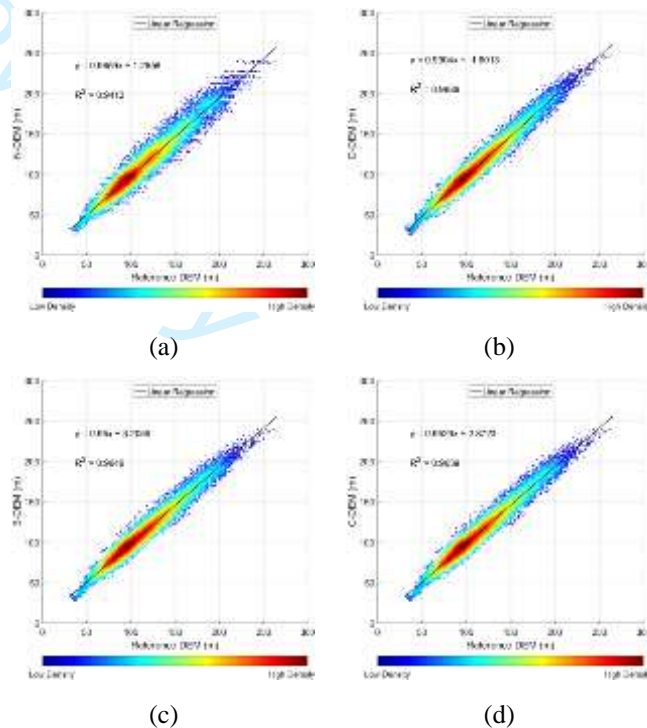Fig. 8. Scatterplots of the reference fine spatial resolution DEM against the downscaled DEMs for the degraded 30 m Nghe An dataset test: (a) the reference DEM and the coarse degraded DEM (N-DEM), (b) the reference DEM and the HNN downscaled DEM (D-DEM), (c) the reference DEM and the bilinear resampled DEM (B-DEM), (d) the reference DEM and the bi-cubic resampled DEM (C-DEM).

(a) (b)

(c) (d)
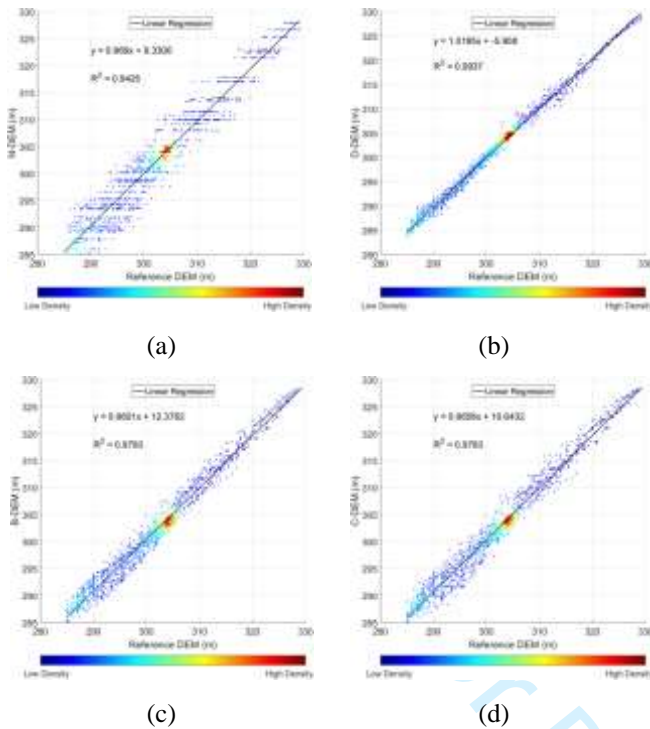
Fig. 9. Scatterplots of the reference fine spatial resolution DEM against the downscaled DEM for the sampled 5 m Lang Son dataset test: (a) the reference DEM and coarse degraded DEM (N-DEM), (b) the reference DEM and the HNN downscaled DEM (D-DEM), (c) the reference DEM and the bilinear resampled DEM (B-DEM), (d) the reference DEM and the bi-cubic resampled DEM (C-DEM).

(a) (b)

(c) (d)

Fig. 10. Scatterplots of the reference fine spatial resolution DEM against the downscaled DEM for the sampled 30 m Dac Ha dataset test: (a) the reference DEM and the coarse degraded DEM (N-DEM), (b) the reference DEM and the HNN downscaled DEM (D-DEM), (c) the reference DEM and the bilinear resampled DEM (B-DEM), (d) the reference DEM and the bi-cubic resampled DEM (C-DEM).
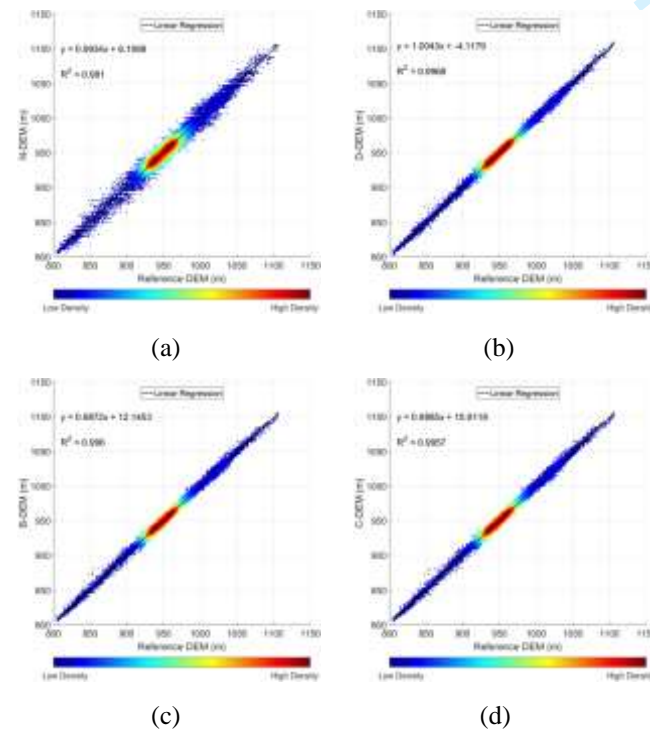
TABLE 4
ROOT MEAN SQUARED ERROR FOR THE PREDICTIONS USING THE BILINEAR RESAMPLING, BI-CUBIC RESAMPLING AND THE HNN DOWNSCALING ALGORITHMS FOR THE LANG SON 5 M DEM

Datasets	Original coarse DEM (m)	Bilinear Resampling (m)	Bi-cubic Resampling (m)	HNN downscaling (m)	Accuracy improvement over coarse DEM (%)
Overall RMSE	2.4571	1.5139	1.6000	0.8493	65.4
CP 1	1.4960	1.2419	1.2912	0.9734	34.9
CP2	1.6962	1.1635	1.1821	0.5120	69.8
CP 3	2.0641	1.4043	1.4791	0.7383	64.2
CP 4	2.2345	1.3591	1.4586	0.7156	68.0
CP 5	2.2705	1.3006	1.3728	0.9587	57.8
CP 6	2.3084	1.7034	1.7805	0.8381	63.7
CP 7	2.0349	1.6198	1.6569	0.8068	60.4
CP 8	2.0325	1.4749	1.5564	0.8032	60.5
CP 9	2.0937	1.2861	1.3578	0.9988	52.3
CP 10	1.9876	1.2374	1.2959	0.9294	53.2
RP 1	1.9569	1.4024	1.4348	0.8798	55.0
RP 2	2.2873	1.6555	1.7196	0.7838	65.7
RP 3	2.3612	1.6712	1.7451	1.1155	52.8
RP 4	1.9510	1.4361	1.5174	0.5897	69.8
RP 5	1.7489	1.4228	1.4657	0.6816	61.0
RP 6	1.7289	1.4081	1.4297	1.1131	35.6
RP 7	1.6217	1.1567	1.2101	0.7876	51.4
RP 8	1.3897	0.8887	0.9730	0.6621	52.4
RP 9	1.4791	0.9317	0.9592	0.5098	65.5
RP 10	1.8042	1.4126	1.4593	0.6564	63.6

*CP stands for Column Profile
*RP stands for Row Profile.

TABLE 3
ROOT MEAN SQUARED ERROR FOR THE PREDICTIONS USING THE BILINEAR RESAMPLING, BI-CUBIC RESAMPLING AND THE HNN DOWNSCALING ALGORITHMS FOR THE NGHE AN SRTM 30 M DEM

Datasets	Original coarse DEM (m)	Bilinear Resampling (m)	Bi-cubic Resampling (m)	HNN downscaling (m)	Accuracy improvement over coarse DEM (%)
Overall RMSE	11.1379	8.8105	8.8736	8.3510	25.0
CP 1	8.5013	6.8408	6.9101	6.4673	23.9
CP 2	9.7106	8.4326	8.4863	8.5069	12.4
CP 3	11.6961	10.7635	10.8141	10.4270	10.9
CP4	10.0198	8.9907	9.0225	8.3592	16.6
CP 5	9.2745	7.0420	7.2130	7.0696	23.8
CP 6	11.5945	9.8018	9.8618	9.7523	15.9
CP 7	9.7925	8.3543	8.4407	8.5220	13.0
RP 1	10.4429	9.8024	9.8357	9.3701	10.3
RP 2	9.9168	8.0953	8.0897	7.6225	23.1
RP 3	10.5144	9.6251	9.6645	9.3598	11.0
RP 4	9.9849	7.7341	7.8310	8.3409	16.5
RP 5	9.8911	8.4770	8.5192	7.6701	22.5
RP 6	8.8079	7.7367	7.7801	7.6159	13.5
RP 7	6.6352	6.4032	6.4005	6.3202	4.7

*CP stands for Column Profile
*RP stands for Row Profile.

The visual comparison of scatterplots in Fig. 7, Fig. 8, Fig. 9, and Fig. 10 also showed the better match between the results of the HNN downscaling and the reference DEM data in comparison with the original coarse DEM and resampling results. In these scatterplots, the two DEM data are considered to be closer if the data points are located closer to the regression line. That means the slope coefficient m is closer to the value of

1 and the intercept coefficient b is closer to the value of 0. The scatterplots of the HNN downscaling results in Fig. 7(b), Fig. 8(b), Fig. 9(b), and Fig. 10(b) showed a closer match between the reference DEM and the HNN downscaled DEM data in comparison with the original coarse DEM data (Fig. 7(a), Fig. 8(a), Fig. 9(a), and Fig. 10(a)) and the bilinear (Fig. 7(c), Fig. 8(c), Fig. 9(c), and Fig. 10(c)) and bi-cubic (Fig. 7(d), Fig. 8(d), Fig. 9(d), and Fig. 10(d)) resampling DEM data. This improvement can be seen most clearly with the 5 m sampled Lang Son and 20 m degraded Nghe An datasets. The data points in the scatterplots in Fig. 7(b) (20 m HNN downscaled DEM) and Fig. 9(b) (5 m HNN downscaled DEM) are distributed very close to (and sometimes exactly on) the best fit line and the best fit line's coefficients in these scatterplots are closer to the value of 1 and 0. Comparing the four datasets, the data points in the scatterplots in Fig. 7(c), Fig. 8(c), Fig. 9 and Fig. 10(c) (bilinear resampled DEM), and Fig. 7(d), Fig. 8(d), Fig. 9(d), and Fig. 10(d) (bi-cubic resampled DEM) are more scattered away from the best fit line than those of the HNN downscaled DEMs.

3) Quantitative assessment

   Coinciding with the result of visual observation, quantitative assessment based on the RMSE (Table 2, Table 3, Table 4, and Table 5) reveals a greater accuracy for the HNN downscaling

TABLE 5
ROOT MEAN SQUARED ERROR FOR THE PREDICTIONS USING THE BILINEAR RESAMPLING, BI-CUBIC RESAMPLING AND THE HNN DOWNSCALING ALGORITHMS FOR THE DAC HA 30 M DEM

Datasets	Original coarse DEM (m)	Bilinear Resampling (m)	Bi-cubic Resampling (m)	HNN downscaling (m)	Accuracy improvement over coarse DEM (%)
Overall RMSE	5.0680	2.3284	2.4218	2.0946	58.67
CP 1	4.0702	2.3434	2.4436	2.2320	45.16
CP 2	4.0203	2.0594	2.2048	1.9625	51.19
CP 3	3.8541	2.0370	2.0956	2.2621	41.31
CP 4	3.5399	2.2395	2.2698	2.3247	34.33
CP 5	3.4595	1.8231	1.9178	1.8204	47.38
CP 6	2.3885	1.3172	1.3603	1.4309	40.09
CP 7	2.6743	1.1377	1.2514	0.9323	65.14
CP 8	2.2896	1.0186	1.1031	0.9520	58.42
CP 9	2.0938	1.0068	1.0624	0.9615	54.08
RP 1	4.6476	1.8714	1.9762	2.5334	45.49
RP 2	4.6907	2.2973	2.3739	2.3246	50.44
RP 3	4.5113	1.7205	1.8051	1.6411	63.62
RP 4	3.6187	1.4932	1.5675	1.4326	60.41
RP 5	3.9713	1.2816	1.4015	1.3186	66.80
RP 6	3.2681	1.0181	1.0540	1.1284	65.47
RP 7	2.8494	1.5355	1.5676	1.6376	42.53
RP 8	3.0366	1.0666	1.0934	1.1509	62.10
RP 9	4.2630	1.9581	2.0194	1.9647	53.91
RP 10	5.2869	2.3473	2.4070	2.8301	46.47

*CP stands for Column Profile
[+]RP stands for Row Profile.

method over the conventional resampling methods for the results of all four datasets. Among the two degraded data, the increase in accuracy is higher for 20 m data. The RMSE for the HNN downscaling DEM is 1.9853 m while the RMSEs for the bilinear and bi-cubic resampling methods are 3.3716 m and 3.3716 m, respectively. Comparing with the RMSE of the original 60 m data, the RMSE of the HNN downscaled 20 m reduced significantly by 71.3% from 6.9326 m to 1.9853 m. For

the Nghe An 30 m degraded test data, the increase in accuracy for HNN downscaling algorithm is not as large as for the 20 m datasets but it is still very convincing with the RMSE decreased by 25% comparing with the original 90 m DEM. The improvement in accuracy for sampled datasets is similar to that of the degraded datasets. The RMSE of 5 m Lang Son data decreased sharply for the HNN downscaling DEM to 0.8493 m from 2.4571 m for the original DEM (65.4%), 1.5139 m for bilinear resampling and 1.6 m for bi-cubic resampling results, respectively. The result for 30 m Dac Ha test is not as impressive as that of 5 m Lang Son data, however, the improvement of DEM accuracy is significant with the RMSE decreased by 50.67% in comparison with the original coarse images. These statistics demonstrate that the proposed HNN method can increase the accuracy of the gridded DEM when it is used to downscale DEM to a finer spatial resolutions. Furthermore, the algorithm in the presented examples seemed to work more effectively with the finer spatial resolution DEMs.

   The increase in accuracy in term of RMSE, along with the profiles, demonstrated the effects of the terrain features on the algorithm. For the 20 m and 30 m datasets in Nghe An, the increase in accuracy between the original and downscaled DEMs was relatively constant. For the 30 m dataset, the increase in accuracy for most profiles was between 10% and for the 5 m sampled Lang Son dataset is more variable with the smallest value of 35% and the largest value of 49%. This is because most of the profiles with a large increase in accuracy of more than 65% (such as column cross-sections 2, 4 and row cross-sections 2, 4, 9) are located in areas of specific terrain such as valley bottoms or the tops of hills. In contrast, the profiles with a smaller increase in accuracy occur mostly on the sides of mountains where the surface of the original (coarse) DEM is relatively close to the reference (fine) DEM. The smaller amount of variation in the increase in accuracy for the 20 m and 30 m degraded datasets and 30 m sampled Dac Ha dataset occurs because most profiles located along many different types of terrain rather than occurring mostly on specific terrain forms.

   The increase in accuracy in term of RMSE, along with the profiles, demonstrated the effects of the terrain features on the algorithm. For the 20 m and 30 m datasets in Nghe An, the increase in accuracy between the original and downscaled DEMs was relatively constant. For the 30 m dataset, the increase in accuracy for most profiles was between 10% and 20%. The range of the increase in accuracy for the 20 m dataset is 20% and between 50% and 70%. The increase in accuracy for the 5 m sampled Lang Son dataset is more variable with the smallest value of 35% and the largest value of 49%. This is because most of the profiles with a large increase in accuracy of more than 65% (such as column cross-sections 2, 4 and row cross-sections 2, 4, 9) are located in areas of specific terrain such as valley bottoms or the tops of hills. In contrast, the profiles with a smaller increase in accuracy occur mostly on the sides of mountains where the surface of the original (coarse)

TABLE 6
LINEAR REGRESSION COEFFICIENTS FOR 20 M NGHE AN AND 30 M NGHE AN RESAMPLED DATASETS, AND THE LANG SON 5 M AND DAC HA 30 M SAMPLED DATASETS.

Datasets		Linear Regression Coefficients				
		m	$|1-m|$	b	$|b|$	R^2
20 m Nghe An dataset	60 m degraded DEM	0.9822	0.0178	2.1147	2.1147	0.9770
	20 m downscaled DEM	0.9981	0.0019	0.2949	0.2949	0.9973
	20 m bilinear resampled DEM	0.9765	0.0235	2.5368	2.5368	0.9951
	20 m bi-cubic resampled DEM	0.9781	0.0219	2.3680	2.3680	0.9948
30 m Nghe An dataset	90 m degraded DEM	0.9659	0.0341	1.2658	1.2658	0.9412
	30 m downscaled DEM	0.9904	0.0096	-1.6013	1.6013	0.9686
	30 m bilinear resampled DEM	0.9500	0.0500	3.2057	3.2057	0.9646
	30 m bi-cubic resampled DEM	0.9529	0.0471	2.8723	2.8723	0.9639
Lang Son dataset	20 m coarse DEM	0.9690	0.0310	9.3306	9.3306	0.9425
	5 m downscaled DEM	1.0195	0.0195	-5.9080	5.9080	0.9937
	5 m bilinear resampled DEM	0.9601	0.0399	12.3782	12.3782	0.9793
	5 m bi-cubic resampled DEM	0.9658	0.0342	10.6432	10.6432	0.9763
Lang Son dataset	90 m coarse DEM	0.9934	0.0066	6.1988	6.1988	0.9810
	30 m downscaled DEM	1.0043	0.0043	-4.1179	4.1179	0.9968
	30 m bilinear resampled DEM	0.9872	0.0128	12.1453	12.1453	0.9960
	30 m bi-cubic resampled DEM	0.9885	0.0115	10.9118	10.9118	0.9959

DEM is relatively close to the reference (fine) DEM. The smaller amount of variation in the increase in accuracy for the 20 m and 30 m degraded datasets and 30 m sampled Dac Ha dataset occurs because most profiles located along many different types of terrain rather than occurring mostly on specific terrain forms.20%. The range of the increase in accuracy for the 20 m dataset is 20% and between 50% and 70%. The increase in accuracy

The similarity of the two DEMs can also be evaluated quantitatively using the linear regression coefficients (m, b) and the correlation coefficient R. Comparing two DEMs, if the elevation of a pixel in the reference dataset is x and the elevation of the corresponding pixel in the comparing dataset is y, the expected perfect fit line should be $y = x$ such that $m = 1$ and $b = 0$. Because the value of m may be greater or smaller than 1 and the value of b may be greater or smaller than 0, comparison between different values of m and b to define the closeness of them to 1 and 0, respectively, sometimes does not make sense. To make more sense for this evaluation, the sub-parameters such as $|1-m|$ and $|b|$ were calculated (Table 6). Accordingly, the smaller values of $|1-m|$ and $|b|$ simultaneously are, the more similar the two datasets are. The third parameter for evaluating the fitting of the two datasets is the correlation coefficient R. The correlation coefficient measures the association between two datasets and, thus, captures the distribution of the data points in the scatterplots around the best fit line. The closer value of R^2 to 1, the more data points are located close to the best fit line. A perfect match between two DEM datasets means that all the data points are located on the identity line ($y = x$) and the coefficient of determination $R^2 = 1$. However, note that it is possible for $R^2 = 1$ where the points lie on the best fit line, but the best fit line does not lie on the 1:1 line. Such as situation indicates bias, which is not measured by R. That means the two datasets are

exactly the same if the value of m is equal to 1, b is equal to 0 and R^2 is equal to 1, simultaneously.

To evaluate the results of the different methods, linear regression models were fitted to the relation between the reference data and the downscaled and resampled datasets (Table 6). The coefficient values show the better fitting of the HNN downscaled DEMs with the reference DEMs than those of the original DEMs, bilinear and bi-cubic resampled DEMs. For all four datasets, the values of parameters m, b and R^2 of the HNN downscaled DEMs are much closer to the values of 1, 0, and 1, respectively, than those of the original, bilinear and bi-cubic resampled DEMs. In case of the Lang Son 5 m resampled dataset, the values $|1-m| = 0.0195$, $|b| = 5.9080$ and $R^2 = 0.9937$ for the HNN downscaled DEM showed greater similarity to the reference DEM than those of the original coarse DEM ($|1-m| = 0.0310$, $|b| = 9.3306$ and $R^2 = 0.9425$), bilinear resampled DEM ($|1-m| = 0.0399$, $|b| = 12.3782$ and $R^2 = 0.9793$) and bi-cubic resampled DEM ($|1-m| = 0.0342$, $|b| = 10.6432$ and $R^2 = 0.9763$). Linear regression statistics for the Dac Ha sampled data also showed the better matching of the downscaled DEM to the reference with $|1-m| = 0.0043$, $|b| = 4.1179$ and $R^2 = 0.9968$ comparing with $|1-m| = 0.0128$, $|b| = 12.1453$ and $R^2 = 0.9960$ for bilinear resampling and $|1-m| = 0.0115$, $|b| = 10.9118$ and $R^2 = 0.9959$ for bi-cubic resampling.

Linear regression coefficients for the 20 m Nghe An degraded dataset showed that the HNN downscaled DEM matches very closely to the reference DEM with $|1-m| = 0.0019$, $|b| = 0.2949$ and $R^2 = 0.9973$ whereas the other downscaled DEMs are very different to the reference DEM. Surprisingly, the comparison also showed that the original coarse DEM with parameters of $|1-m| = 0.0178$ and $|b| = 2.1147$ is generally more matched to the reference DEM than

the resampled DEMs with $|1 - m| = 0.0235$ and $|b| = 2.5368$, and $|1 - m| = 0.0219$ and $|b| = 2.3680$ for bilinear and bi-cubic resampled DEMs, respectively. However, more data points of the bilinear ($R^2 = 0.9951$) and bi-cubic ($R^2 = 0.9948$) resampled DEMs are distributed close to the best fit line than those of the original 20 m DEM ($R^2 = 0.9770$).

For the 30 m degraded dataset, the increase in prediction precision of the HNN downscaling is clearly seen when comparing the linear regression parameters of the three methods. Although the coefficient of determination of the HNN downscaling result ($R^2 = 0.9686$) is just slightly larger than those of the bilinear ($R^2 = 0.9646$) and bi-cubic ($R^2 = 0.9639$) methods, the best fit lines of the datasets showed less bias of the HNN downscaled DEM data with the reference data ($|1 - m| = 0.0096$ and $|b| = 1.6013$) than those of the bilinear ($|1 - m| = 0.0500$ and $|b| = 3.2057$) and bi-cubic ($|1 - m| = 0.0471$ and $|b| = 2.8723$) resampling data.

Comparing the slope parameter m and intercept parameter b of the best fit lines of all four datasets, it is clear that all the slope parameters m of the resampled DEMs are smaller than 1 and the intercept parameters b are larger than 0. This means that for locally-low places (usually the bottom of valleys) the pixels of the DEM data produced by these methods are likely to be higher than the corresponding pixels in the reference DEM. Conversely, for locally-high places such as the top of hills or mountain ridges, the elevation of the pixels in the resampled DEM data is likely lower than that of the corresponding pixels in the reference image. This is due to the smoothing effect (referred to as conditional bias where highs are under-predicted and lows are over-predicted) and can be reduced using the HNN downscaling. The evidence for this is the values of the four pairs of m and b values for the HNN downscaling method for the 20 m ($m = 0.9981$, $b = 0.2949$) and 30 m ($m = 0.9904$, $b = -1.6013$) degraded DEMs and 5 m ($m = 1.0195$, $b = -5.9080$) and 30 m ($m = 1.0043$, $b = -4.1179$) sampled DEMs. These best fit lines are very close to the 1:1 line with $m = 1$, and $b = 0$. Even for the 5 m dataset, the HNN downscaling method has a tendency to produce elevation values in low elevation areas that are slightly *lower* and elevation values in high elevation areas that are slightly *higher* than those of the reference DEM. This can be explained by the effect of the *elevation constraint* of the HNN downscaling model. This effect is crucial, as it demonstrates that the HNN approach works not because it is an alternative spatial smoother that captures more of the salient information in the coarse resolution data, but explicitly because it imposes a pixel-level constraint on the predictions such that extremes tend to be more closely honoured. In other words, the structure of the HNN method (formulated as a within- and across-pixel smoothing goal and pixel-level constraint) means that it brings a specific advantage that other commonly applied resampling methods do not.

IV. CONCLUSION

A new method for increasing the spatial resolution and accuracy of gridded DEMs was proposed and demonstrated comprehensively using data with different DEM spatial resolutions and characteristics. The newly proposed downscaling algorithm was formulated based on the Hopfield neural network (HNN) with a spatial dependence maximization goal function and an elevation constraint. Tests of the proposed algorithm were implemented on two types of elevation datasets; 20 m and 30 m degraded DEMs in Nghe An province, Vietnam, a 5 m sampled DEM in Lang Son province (from ground surveying elevation data), and 30 m sampled DEM in Dac Ha, Kontum Province, Vietnam (generated from the contour lines). The new method was evaluated against two existing and commonly applied methods;:bilinear and bi-cubic resampling.

The test results revealed a sharp increase in accuracy for the HNN downscaled gridded DEMs in comparison with the original (coarse) gridded DEM, and the bilinear and bi-cubic resampling downscaled DEMs. Visual assessment revealed the greater similarity of the HNN downscaled DEMs with the reference DEM than the DEMs generated by bilinear and bi-cubic resampling. Quantitative accuracy assessment based on the RMSE revealed an increase in DEM accuracy for the HNN downscaling algorithm over the bilinear and bi-cubic resampling methods. The RMSE of the downscaled DEMs decreased by approximately 71%, 25%, 65%, and 58% for the 20 m and 30 m degraded DEMs in Nghe An province, 5 m sampled DEM in Lang son province, and 30 m sampled DEM in Dac Ha, Vietnam, respectively. The RMSE values of the HNN downscaled DEM were lower in comparison with those of the bilinear and bi-cubic resampling methods, especially for the 5 m and 20 m datasets.

Further evaluation was also implemented using linear regression of the original fine spatial resolution DEM against the original, the HNN downscaled DEM, and the bilinear and bi-cubic resampled DEMs, particularly focusing on the coefficients m, b and R^2. Analysis of these parameters showed that the HNN downscaled DEMs was closer to the reference DEMs than the original DEM and those produced using the bilinear and bi-cubic resampling methods.

Visual and quantitative assessment showed that the HNN downscaling algorithm performed more accurately for some specific terrain features such as valley bottoms or the crests of ridges. The RMSEs of profiles located mostly in these terrain features decreased by about 20% (i.e., improved more) compared with those of the profiles occurring mostly on mountain sides or flat areas. This improvement can be attributed to the effects of the combination of the elevation constraint with the spatial dependence maximization functions in the HNN approach. That is, the specific formulation of the HNN method brings structural advantages to the DEM downscaling task that cannot be achieved using commonly applied spatial resampling methods.

REFERENCES

[1] Siddharth Saksena and Venkatesh Merwade, "Incorporating the effect of DEM resolution and accuracy for improved flood inundation mapping," *Journal of Hydrology*, vol. 530, pp. 180–194, 2015.

[2] A Sivasena Reddy and M Janga Reddy, "Evaluating the influence of spatial resolutions of DEM on watershed runoff and sediment yield using SWAT," *Journal of Earth System Science*, vol. 124, no. 7, pp. 1517–1529, 2015.

[3] Ling Bian and Rachael Butler, "Comparing Effects of Aggregation Methods on Statistical and Spatial Properties of Simulated Spatial Data," *Photogrammetric Engineering & Remote Sensing*, vol. 65, no. 1, pp. 73-84, 1999.

[4] Zhengyong Zhao et al., "Impacts of Accuracy and Resolution of Conventional and LiDAR Based DEMs on Parameters Used in Hydrologic Modeling," *Water Resources Management*, vol. 24, no. 7, pp. 1363-1380, 2010.

[5] Kang-tsung Chang and Bor-wen Tsai, "The Effect of DEM Resolution on Slope and Aspect Mapping," *Cartography and Geographic Information Systems*, vol. 18, no. 1, pp. 69-77, 1991.

[6] P.V. Bolstad and T. Stowe., "An evaluation of DEM accuracy: elevation, slope, and aspect," *Photogrammetric Engineering and Remote Sensing*, vol. 60, pp. 1327-1332, 1994.

[7] I. Chaubey, A. S. Cotter, T. A. Costello, and T. S. Soerens, "Effect of DEM data resolution on SWAT output uncertainty," *Hydrological Processes*, vol. 19, no. 3, pp. 621–628, Feb. 2005.

[8] Kishan Singh Rawat, Gopal Krishna, Amresh Mishra, Jitendra Singh, and Shashi Vind Mishra, "Effect of DEM data resolution on low relief region sub-watershed boundaries delineating using of SWAT model and DEM derived from CARTOSAT-1 (IRS-P5), SRTM and ASTER," *Journal of Applied and Natural Science*, pp. 144-151, 2014.

[9] Baxter E. Vieux, "DEM Aggregation and Smoothing Effects on Surface Runoff Modeling," *Journal of Computing in Civil Engineering*, vol. 7, no. 3, pp. 310--338, Jan. 1993.

[10] RF Vazquez and J Feyen, "Assessment of the effects of DEM gridding on the predictions of basin runoff using MIKE SHE and a modelling resolution of 600m," *Journal of Hydrology*, vol. 334, no. 1-2, pp. 73–87, 2007.

[11] J. M. Schoorl, M. P. W. Sonneveld, and A. Veldkamp, "Three-dimensional land landscape process modelling: the effect of DEM resolution," *Earth Surface Processes and Landforms*, vol. 25, pp. 1025-1034, 2000.

[12] Jing Li and David Wong, "Effects of DEM sources on hydrologic applications," *Computers, Environment and Urban Systems*, vol. 34, no. 2, pp. 251–261, 2010.

[13] Mauro Sulis, Claudio Paniconi, and Matteo Campores, "Impact of grid resolution on the integrated and distributed response of a coupled surface–subsurface hydrological model for the des Anglais catchment, Quebec," *Hydrological Processes*, pp. pp. 1853–1865, 2011.

[14] Michael P. Smith, A-Xing Zhub, James E. Burt, and Cynthia Stiles, "The effects of DEM resolution and neighborhood size on digital soil survey," *Geoderma*, vol. 137, pp. 58-69, 2006.

[15] Wen-Ling Kuo et al., "Effect of grid size on runoff and soil moisture for a variable-source-area hydrology model," *Water Resources Research*, vol. 35, no. 11, pp. 3419-3428, 1999.

[16] Qinghua Guo, Wenkai Li, Hong Yu, and Otto Alvarez, "Effects of Topographic Variability and Lidar Sampling Density on Several DEM Interpolation Method," *Photogrammetric Engineering & Remote Sensing*, vol. 76, no. 6, pp. 701-712, 2010.

[17] John P. Wilson, "Digital terrain modeling," *Geomorphology*, vol. 137, no. 1, pp. 107-121, 2012.

[18] S. Rapinel, L. Hubert-Moy, B. Clément, Nabucet J., and C. Cudennec, "Ditch network extraction and hydrogeomorphological characterization using LiDAR-derived DTM in wetlands," *Hidrology Research*, vol. 46, no. 2, pp. 276-290, 2015.

[19] Xiaoye Liu, "Airborne LiDAR for DEM generation: some critical issues," *Progress in Physical Geography*, vol. 32, no. 1, pp. 31-49, 2008.

[20] David Kidner, Mark Dorey, and Derek Smith, "What's the point? Interpolation and extrapolation with a regular grid DEM," in *GeoComputation Conference Proceedings*, Virginia, 1999, pp. CD-ROM Procedings.

[21] Simon Wu, Jonathan Li, and G.H. Huang, "A study on DEM-derived primary topographic attributes for hydrologic applications: Sensitivity to elevation data resolution," *Applied Geography*, vol. 28, pp. 210–223, 2008.

[22] Wenzhong Shi, Bin Wang, and Yan Tian, "Accuracy Analysis of Digital Elevation Model Relating to Spatial Resolution and Terrain Slope by Bilinear Interpolation," *Mathematical Geosciences*, vol. 6, no. 5, pp. 445–481, 2014.

[23] B. Dixon and J. Earls, "Resample or not? Effects of resolution of DEMs in watershed modeling," *Hydrological Processes*, vol. 23, pp. 1714–1724, 2009.

[24] L. E. Band and I. D. Moore, "Scale: Landscape attributes and geographical information systems," *Hydrologic Processes*, vol. 9, pp. 401-422, 1995.

[25] R. Jana, T.V. Reshmidevi, P.S. Aruna, and T.I. Eldho, "An enhanced technique in construction of the discrete drainage network from low-resolution spatial database," *Computers & Geosciences*, vol. 33, no. 6, pp. 717-727, 2007.

[26] Gyozo Jordan, "Adaptive smoothing of valleys in DEMs using TIN interpolation from ridgeline elevations: An application to morphotectonic aspect analysis," *Computers & Geosciences*, vol. 33, pp. 573–585, 2007.

[27] C.U. Paredes-Hernández, N.J. Tate, K.J. Tansey, P.F. Fisher, and W.E. Salinas-Castillo, "Increasing the Accuracy of Low Spatial Resolution Digital Elevation

Models using Geostatistical Conflation," , Zurich, Switzerland, 2010.

[28] Yunwei Tang et al., "A multiple-point geostatistical method for digital elevation models conflation," in *Geoscience and Remote Sensing Symposium (IGARSS), 2014 IEEE International* , Quebec City, QC, Canada, 2014.

[29] Brian Atkins et al., "Computerized method for improving data resolution," US 6075926 A, 2000.

[30] P. M. Atkinson, "Mapping sub-pixel boundaries from remotely sensed image," in *Innovation in GIS*, Kemp, Ed. London: Taylor and Francis, 1997, vol. 4.

[31] Y. F. Su, G. M. Foody, A. M. Muad, and K. S. Cheng, "Combining Hopfield Neural Network and Contouring Methods to Enhance Super-Resolution Mapping," *IEEE Journal of Selected Topics in Applied Earth Observations and Remote Sensing*, vol. 5, no. 5, pp. 1403 - 1417, 2012.

[32] M.W. Thornton, P.M. Atkinson, and D.A. Holland, "Sub-pixel mapping of rural land cover objects from fine spatial resolution satellite sensor imagery using super-resolution pixel-swapping," *International Journal of Remote Sensing*, vol. 27, no. 3, pp. 473-491, 2006.

[33] Chang Huang, Yun Chen, and Jianping Wu, "DEM-based modification of pixel-swapping algorithm for enhancing floodplain inundation mapping," *International Journal of Remote Sensing*, vol. 35, no. 1, pp. 365-381, 2014.

[34] Liguo Wang and Qunming Wang, "Subpixel Mapping Using Markov Random Field With Multiple Spectral Constraints From Subpixel Shifted Remote Sensing Images," *IEEE Geosciences and Remote Sensing Letters*, vol. 10, no. 3, pp. 598 - 602, May 2013.

[35] A. J. Tatem, H. G. Lewis, P. M. Atkinson, and M. S. Nixon, "Multi-class land cover mapping at the sub-pixel scale using a Hopfield neural network," *International Journal of Applied Earth Observation and Geoinformation*, vol. 3, pp. 184-190, 2001.

[36] Q. M. Nguyen, P. M. Atkinson, and H. G Lewis, "Super-resolution mapping using Hopfield neural netwok with panchromatic image," in *Asian Conference on Remote Sensing ACRS, CD-ROM*, Hanoi, 2005.

[37] A.M. Muad and G.M. Foody, "Super-resolution mapping using multiple observations and Hopfield neural network," in *Proceedings of the SPIE Remote Sensing: Image and Signal Processing for Remote Sensing XVI*, Toulouse, France, 2010.

[38] Xiaodong Li, Feng Ling, Yun Du, Qi Feng, and Yihang Zhang, "A spatial–temporal Hopfield neural network approach for super-resolution land cover mapping with multi-temporal different resolution remotely sensed images," *ISPRS Journal of Photogrammetry and Remote Sensing*, vol. 93, pp. 76-87, 2014.

[39] Qunming Wang, Wenzhong Shi, Peter M. Atkinson, and Zhongbin Li, "Land Cover Change Detection at Subpixel Resolution With a Hopfield Neural Network ,"

IEEE Journal of Selected Topics in Applied Earth Observations and Remote Sensing , vol. 8, no. 3, pp. 1339 - 1352 , 2015.

[40] Quang Minh Nguyen, Van Duong Do, P.M. Atkinson, and H.G.Lewis, "Downscaling Multispectral Imagery Based on the HNN Using Forward Model," in *7th FIG Regional Conference on Spatial Data Serving People: Land Governance and the Environment-Building the Capacity*, Hanoi, 2009.

[41] Quang Minh Nguyen, Peter M. Atkinson, and Hugh G. Lewis, "Super-resolution mapping using Hopfield Neural Network with panchromatic imagery," *International Journal of Remote Sensing*, vol. 32, no. 21, pp. 6149-6176, 2011.

[42] David W. Tank and John J. Hopfield, "Simple " Neural" Optimization Networks: An A/D Converter, Signal Decision Circuit, and 'a Linear Programming Circuit," *IEEE Transactions on Circuits and Systems, Vol. Cas-33, No. 5, May 1986*, vol. 33, no. 5, pp. 533-541, 1986.

[43] Ken Whitehead and Chris H. Hugenholtz, "Applying ASPRS Accuracy Standards to Surveys from Small Unmanned Aircraft Systems (UAS)," *Photogrammetric Engineering and Remote Sensing*, vol. 81, no. 10, pp. 787-793, 2015.

[44] ASPRS, "ASPRS Accuracy Standards for Digital Geospatial Data," *Photogrammetric Engineering & Remote Sensing*, vol. 81, no. 2, pp. A1-A26, 2015.

[45] Ugur Alganci, Baris Besol, and Elif Sertel, "Accuracy Assessment of Different Digital Surface Models," *ISPRS International Journal of Geo-information*, vol. 2, no. 114, 2018.

[46] Phaedon C. Kyriakidis, Ashton M. Shortridge, and Michael F. Goodchild, "Geostatistics for conflation and accuracy assessment of digital elevation models," *International Journal of Geographical Information Science*, vol. 13, no. 7, pp. 677-707, Jan. 1999.

[47] Stefan Kienzle, "The Effect of DEM Raster Resolution on First Order, Second Order and Compound Terrain Derivatives," *Transaction in GIS*, vol. 8, no. 1, pp. 83-111, 2004.

[48] P.M. Atkinson, E. Pardo-Iguzquiza, and M. Chica-Olmo, "Downscaling Cokriging for Super-Resolution Mapping of Continua in Remotely Sensed Images," *IEEE Transactions on Geoscience and Remote Sensing*, vol. 46, no. 2, pp. 573 - 580, 2008.